frontiers | Frontiers in Earth Science

TYPE Original Research
PUBLISHED 09 March 2023
DOI 10.3389/feart.2023.1135901

OPEN ACCESS

EDITED BY
Shangfeng Chen,
Institute of Atmospheric Physics (CAS), China

REVIEWED BY
R. V Krishnamurthy,
Western Michigan University, United States
Zhibiao Wang,
Institute of Atmospheric Physics (CAS), China

*CORRESPONDENCE
Haiwei Zhang,
zhanghaiwei@xjtu.edu.cn

SPECIALTY SECTION
This article was submitted to Interdisciplinary Climate Studies, a section of the journal Frontiers in Earth Science

RECEIVED 02 January 2023
ACCEPTED 27 February 2023
PUBLISHED 09 March 2023

CITATION
Bao Y, Zhang H, Niu X, Zhang R, Lu J, Meng B, Lu J, Tan L, Cai Y and Cheng H (2023), Seasonal variations and controlling factors of speleothem multi-proxy in southeastern China: Implications for the reconstruction of precipitation seasonality.
Front. Earth Sci. 11:1135901.
doi: 10.3389/feart.2023.1135901

Seasonal variations and controlling factors of speleothem multi-proxy in southeastern China: Implications for the reconstruction of precipitation seasonality

Yanyan Bao[1], Haiwei Zhang[1,2,3]*, Xiaowen Niu[1], Rui Zhang[1], Jing Lu[1], Binglin Meng[1], Jiayu Lu[4], Liangcheng Tan[2], Yanjun Cai[1,2] and Hai Cheng[1,2,3]

[1]Institute of Global Environmental Change, Xi'an Jiaotong University, Xi'an, China, [2]State Key Laboratory of Loess and Quaternary Geology, Institute of Earth Environment, Chinese Academy of Sciences, Xi'an, China, [3]Key Laboratory of Karst Dynamics, MLR, Institute of Karst Geology, CAGS, Guilin, China, [4]Think Tank of Coastal Development, Yancheng Teachers University, Yancheng, China

Precipitation in southeastern China exhibits strong seasonal variability, which significantly impacts local agricultural production and social development. However, the reconstruction of precipitation seasonality has been limited by the lack of precisely dated high-resolution paleoclimatic records. This study presents seasonal-scale multi-proxy records (trace elements: Mg/Ca, Sr/Ca Ba/Ca and stable isotopes: $\delta^{18}O$ and $\delta^{13}C$) of a modern (1810–2009 AD) annually laminated stalagmite (EM1) from E'Mei Cave, Jiangxi Province in southeastern China. Comparative analysis of observation data with meteorological and simulation data shows that the seasonal variation of EM1 $\delta^{18}O$, derived from precipitation $\delta^{18}O$, is mainly controlled by the large-scale circulation and precipitation seasonality on an interannual timescale. The seasonal EM1 $\delta^{18}O$ variation is controlled by the seasonal precipitation $\delta^{18}O$, however, the most negative values of EM1 $\delta^{18}O$ are higher than those of simulated calcite $\delta^{18}O$ and the average amplitude of the seasonal variation of EM1 $\delta^{18}O$ (~1.93‰) is much smaller than that of simulated calcite $\delta^{18}O$ (~9.72‰) because of evaporation and mixing of waters in the epikarst system. On the decadal timescales, variations of $\delta^{13}C$, Mg/Ca, Sr/Ca, and Ba/Ca were found to be strongly correlated, consistent with the variation of the local dry/flood index, indicating a common influencing factor of local hydroclimate change. However, their seasonal phase relationships vary between strong and weak summer monsoon conditions. We find a strong covariation between Mg/Ca and $\delta^{13}C$ with Sr/Ca and Ba/Ca during the strong monsoon period (1951–1976), and they are in antiphase with seasonal $\delta^{18}O$ variation. However, the seasonal variations of Sr/Ca and Ba/Ca transformed to dominantly antiphase with Mg/Ca and $\delta^{13}C$ during the weak monsoon period (1977–1991 AD). Therefore, we suggest that Mg/Ca and $\delta^{13}C$ are dominantly controlled by the local hydroclimate changes on seasonal timescales but Sr/Ca and Ba/Ca might have been affected by complex processes in the epikarst under different hydrothermal configuration conditions. The findings indicate the potential of the variation of the seasonal phase relationships between multi-

proxy records in reconstructing precipitation seasonality changes under different hydrothermal backgrounds.

KEYWORDS

precipitation seasonality, stalagmite, stable isotopes, trace elements, multi-proxy, paleoclimate

1 Introduction

In recent years, with the rapid development of high resolution sampling methods and modern analysis techniques, many studies based on high-resolution stalagmite proxies have improved our understanding of climate change on the annual-decadal scales (Yadava et al., 2004; Baldini et al., 2005; Mattey et al., 2008; Cai et al., 2010; Jex et al., 2010; Orland et al., 2012; Baker et al., 2015; Lin et al., 2021). These studies focused on the analysis of stalagmite stable oxygen and carbon isotope ($\delta^{18}O$ and $\delta^{13}C$) records, which not only provided important insights into climate-driven mechanisms but also provided more in-depth knowledge on the climatic significance of stalagmite stable isotopes as a climate index. However, the reconstruction of seasonally-resolved hydroclimate variability has generally proven difficult as seasonal resolution climate information is difficult to extract from as most stalagmites because of their slow growth rate. Furthermore, the main influencing factors of stalagmite $\delta^{18}O$ are disparate in different regions on different timescales. For instance, cave monitoring in monsoonal China shows that the seasonal variation of precipitation/modern carbonate $\delta^{18}O$ in some regions has no significant relationship with rainfall amount (Duan et al., 2016). Speleothem $\delta^{18}O$ in subtropical Brazil is dominantly related to the variation of moisture source but not rainfall amount (Francisco et al., 2005). Speleothem $\delta^{18}O$ in southeastern China might be largely controlled by changes in moisture source on seasonal timescales (Tian et al., 2021) and influenced by precipitation seasonality, moisture source, and integrated regional convection on the interannual to decadal timescales (Zhang et al., 2019; Zhang et al., 2020; Lu et al., 2021; Zhang et al., 2021). Different from the $\delta^{18}O$ proxy, speleothem trace element concentrations and ratios are likely to be dependent on local hydroclimate conditions and epikarst systems (Cruz et al., 2007; Fairchild and Treble, 2009; Ban et al., 2018; Tan and Lin, 2020). The climatic explanation of trace elements should emphatically consider the influences of local rainfall on dissolution, recharge, and precipitation processes in epikarst systems (Fairchild et al., 2000; Karmann et al., 2007). Trace elements in speleothems are primarily derived from overlying soil and bedrock (Ban et al., 2018), with some contribution from atmospheric aerosol inputs (Tadros et al., 2019). A series of physical and chemical processes in epikarst zones, including prior aragonite precipitation (PAP), prior calcite precipitation (PCP), incongruent calcite dissolution (ICD) and water–rock interaction (WRI, involving calcite/dolomite recrystallization or inconsistent dissolution of dolomite), residence time of seepage water, mixing of fresh and old water, dilution effect and piston flow of fissure water, play complex but potentially important roles in the trace element ratios of speleothems (Fairchild et al., 2000; Tooth and Fairchild, 2003; Fairchild et al., 2006; Orland et al., 2014; Treble et al., 2015; Zhang and Li, 2019).

In addition, Mg incorporation into calcite may be affected by temperature in some regions (Day and Henderson, 2013; Koltai et al., 2017). Crystal growth rate may influence Sr incorporation into speleothems (Reeder, 1995; Gabitov and Watson, 2006; Tan et al., 2014a). Therefore, analyzing various climate proxy indicators of stalagmite, such as stable isotopes and trace elements, is particularly important for establishing a high-resolution paleoclimate record from stalagmite, which can not only improve the accuracy of the results but also help in distinguishing different mechanisms of trace elements through a multi-proxy approach for establishing reliable seasonal resolution cave records (Johnson et al., 2006; Baldini et al., 2012; Oster et al., 2012; Vansteenberge et al., 2020).

Located in the southern shore of the lower-middle reaches of the Yangtze River, China, northern Jiangxi Province is a crucial production base of grain, cotton, and oil. In the region, spring rain and Meiyu prevail in early summer, but summers in July and August are dry and hot. This seasonally variable precipitation dominantly leads frequent flood and drought events, leading to climate disaster events that seriously affect the lives of local people and hinder the development of agriculture and social economy (Ding et al., 2020). This study analyzed the seasonal variation and phase relation between $\delta^{18}O$, $\delta^{13}C$ and Mg/Ca, Sr/Ca, and Ba/Ca using an annually laminated stalagmite (EM1), collected from E'mei Cave in northern Jiangxi. Combined with accurate seasonal-resolution multi-proxy records of EM1 in recent decades and meteorological data, the influencing factors of these stalagmite proxies in seasonal cycles and their hydro climatic implications were explored. This study is expected to provide suggestions and references for the reconstruction of high-resolution paleoclimate change records in this region.

2 Cave setting and sample

2.1 Cave setting

E'mei Cave (115°29′44″E, 29°33′18″N, 53 m a.s.l.) is located in Henggang Town of Ruichang City, northern Jiangxi Province (Figure 1A). The thickness of the cave roof is approximately 10–30 m.

The study area is dominated by subtropical humid and monsoon climate with strong rainfall seasonality. Spring persistent rain (SPR) lasts from March to May, and the Meiyu period with high temperature and heavy rainfall occurs in June. In contrast, precipitation significantly declines from July to August under the control of the western Pacific subtropical high, which is reflected as high temperature and little rainfall. Precipitation is the lowest during the period from autumn to winter. According to instrumental data (1951–2010 AD) from the Jiujiang meteorological station near E'mei Cave (~50 km from the cave), the region has an annual mean precipitation of 1426.9 mm and an annual mean temperature of 17.5°C. The spring (March to May) and summer (June to August) precipitation account for 35.8% and 34.6% of the annual precipitation, respectively. According to data from the nearest

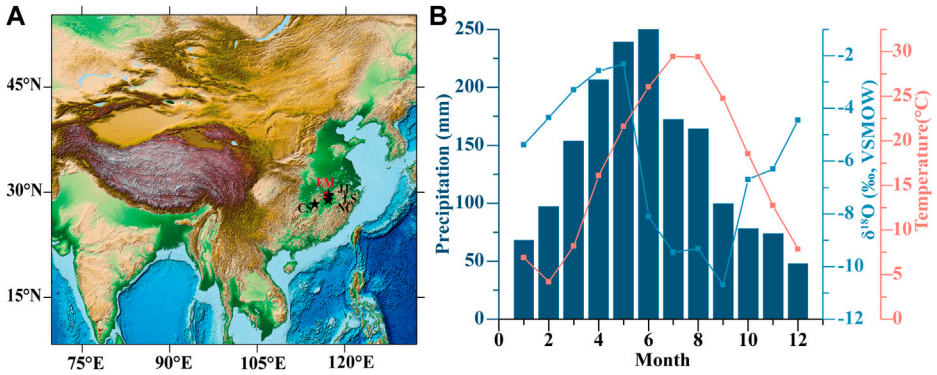

FIGURE 1
Cave location and climatic conditions of the study area. **(A)** Location of E'mei cave and the Jiujiang and Changsha meteorological stations (the red circle indicates E'mei cave (EM), and the black stars indicate the Changsha (CS), Jiujiang (JJ), Lushan (LS) and Nanchang (NC) meteorological stations); **(B)** monthly average precipitation (dark blue bars) and temperature (pink curve) from three stations (Jiujiang, Lushan and Nanchang) from 1951 to 2010 AD and monthly mean precipitation $\delta^{18}O$ at the GNIP Changsha site from 1988 to 1992 AD (blue curve).

Global Network for Isotopes in Precipitation (GNIP) station (Changsha station, ~100 km west of E'mei Cave) during 1988–1992 AD, March-May precipitation (Spring rain) $\delta^{18}O$ values are higher and June-September precipitation (East Asian summer monsoon precipitation) $\delta^{18}O$ values are lower (Figure 1B).

2.2 Sample

A rapidly growing calcitic stalagmite (EM1) of 60 mm in height was collected in December 2009 from an active drip site located ~150 m behind the entrance of E'mei Cave. The top of EM1 is smooth.

The sample was halved along its growth axis and then polished. The polished profile shows continuous laminations; the annual growth laminae are all clearly visible to the naked eye, alternating between translucent, dense sub-layers (TDSL) and white, porous sub-layers (WPSL) (Genty and Quinif, 1996; Tan et al., 2014b) (Supplementary Figure S1). X-ray diffraction (XRD) analyses suggest that the mineral composition of EM1 is pure calcite.

3 Methods and data

3.1 Chronology

Four sub-samples were drilled from polished sections of EM1 using a carbide dental drill for ^{230}Th dating. These subsamples were dated on a Multi-Collector Inductively Coupled Plasma Mass Spectrometry at the Institute of Global Environmental Change, Xi'an Jiaotong University. The laminae of EM1 were counted according to the scan image using a confocal laser fluorescent microscope at the State Key Laboratory for Manufacturing Systems Engineering, Xi'an Jiaotong University. The age model of EM1 was established by combining the ^{230}Th dating results, $\delta^{18}O$ cycle counting, and annual lamina counting. Further details on the age model are provided by Zhang et al. (2018).

3.2 Thin section, stable-isotope, and trace-element analyses

In order to minimize the sampling error, a 20.4 mm-long section (3.5–23.9 mm from the top) of EM1 with very clear annual growth laminae was selected (Supplementary Figure S1). Each annual lamina of this section consists of a translucent, dense and white, porous sub-layer couplet. The growth laminae are quite parallel with less visible pores. A thin section (0–28.5 mm from the top) was also prepared and examined using the Zeiss Axioscope5 microscope.

A total of 204 sub-samples were milled using a high-resolution Micromill device at an interval of 0.1 mm at 3.5–23.9 mm from the top of the polished EM1 profile. The correspondence relationship between each subsample and translucent-white couplet was recorded during the sampling process. Each subsample was divided into two parts for analyses: one part was measured for $\delta^{18}O$ and $\delta^{13}C$ using a Delta V isotope ratio mass spectrometer connected with a Kiel-IV system at Xi'an Jiaotong University and the other part was analyzed for Mg/Ca, Sr/Ca, and Ba/Ca using the Agilent 5110 ICP-OES at the Institute of Earth Environment, Chinese Academy of Sciences. The laboratory standard TTB1 was analyzed after every 10 subsamples to ensure the stability of the stable isotope data. The analytical precision of the $\delta^{18}O$ and $\delta^{13}C$ analyses was 0.07‰ and 0.05‰ (1σ), respectively. All isotopic values are reported in the δ notation relative to the Vienna Pee Dee Belemnite (VPDB) standards. Throughout the trace element measurements, the subsample was dissolved in 5% nitric acid in cleaned centrifuge tubes. A standard sample was inserted after every 5 subsamples and a set of standard samples was inserted after every 15 subsamples for calibration. The relative standard deviations (RSD) were less than 5% for Mg/Ca, Sr/Ca, and Ba/Ca.

3.3 Instrumental data

Average monthly precipitation and temperature data from three near meteorological stations (Jiujiang, Lushan and Nanchang) for the period 1951–2010 AD were obtained from the National Climate

Center (NCA, http://ncc.cma.gov.cn). The D/F index records of Jiujiang region was reconstructed from drought and flood events during spring, summer, and autumn recorded in historical literature, reflecting the local precipitation variation. Monthly precipitation $\delta^{18}O$ data (1988–1992 AD) from the GNIP Changsha stations were obtained from the GNIP (http://www.iaea.org/). Both Changsha station and the study area are located in the spring persistent rain area, their precipitation $\delta^{18}O$ variabilities are consistent (Zhang et al., 2020). Monthly simulated $\delta^{18}O$ data of precipitation (1979–2015 AD) were acquired from a water isotope-permitting general circulation model (IsoGSM) (Yoshimura et al., 2008). IsoGSM has been proven to be capable of producing reliable data for eastern China (Zhang et al., 2020). A comparison between the precipitation $\delta^{18}O$ data (1988–1992 AD) from the GNIP Changsha station and those from IsoGSM simulation showed consistent variations, with a significantly positive correlation [r=0.754; 95% confidence interval (0.614; 0.848)], although the amplitude of the IsoGSM simulated $\delta^{18}O$ was slightly smaller than that of the GNIP observation data (Supplementary Figure S2). Multivariate El Nino-Southern Oscillation Index (MEI) and West Pacific Subtropical High (WPSH) data (1951–1990 AD) were obtained from the Earth System Research Laboratory, National Oceanic & Atmospheric Administration (NOAA) (http://www.cdc.noaa.gov/people/klaus.wolter/MEI). The Pacific Decadal Oscillation (PDO) Index (1951–1990 AD) was also obtained from NOAA (http://www.ncdc.noaa.gov/teleconnections/pdo).

3.4 Water-calcite fractionation and data processing

Under isotope equilibrium fractionation, the $\delta^{18}O$ values of calcite are mainly determined from the $\delta^{18}O$ values of drip water and cave temperature, while the $\delta^{18}O$ values of drip water are derived from the $\delta^{18}O$ of precipitation. In order to calculate the fraction of stalagmite $\delta^{18}O$ attributable to precipitation $\delta^{18}O$, the temperature dependent oxygen isotope fractionation factor between calcite and water established by Kim and O 'Neil (1997) was applied (Equation 1) (Kim and O 'Neil., 1997).

$$\delta^{18}O_{calcite}[VPDB] = \delta^{18}O_{drip\ water}[VPDB] + 18.03\left(\frac{10^3}{T}\right) - 32.42 \quad (1)$$

Where T is the absolute temperature in K (T=273+t°C), t is average annual temperature of the cave in °C. In this study, the IsoGSM simulated precipitation $\delta^{18}O$ was used as drip water $\delta^{18}O$. It should be noted that the unit of precipitation $\delta^{18}O$ is relative to the standard mean ocean water (VSMOW) and the unit of speleothem $\delta^{18}O$ is relative to Pee Dee Belemnite (VPDB), and they need to be transformed into a consistent unit (Equation 2).

$$\delta^{18}O[VPDB] = \left(\delta^{18}O[VSMOW] - 30.864\right)/1.030864 \quad (2)$$

In order to better analyze the seasonal variations of trace element ratios and stable isotopes, the long-term trend of each record was removed using a data detrending method. PearsonT3 was used to calculate the linear Pearson correlation coefficient between different records, which provides the valid corrected 95% confidence intervals in the case of autocorrelation. Beyond that, the confidence interval can be used as a significance test by verifying whether it contains zero.

4 Results

4.1 Growth lamina characteristic

EM1 consists of couplets of alternating TDSL and WPSL under natural light (Figure 2). WPSL corresponds to the opaque layer under transmitted light and it is weak to the strong luminescence band under fluorescence (Figure 2). WPSL has a higher abundance of opaque particles under transmitted and cross-polarized light. These particles glow under fluorescence and may be clay-like impurities or organic matter (Figures 2B,C). Several wide fluorescent layers include multiple extremely thin fluorescent sublayers (Figure 2C). The thin-section image in Figure 2A shows that both sub-layers are composed of typical columnar and fibrous calcite crystalline structures under cross-polarized light.

4.2 Stable isotopes

EM1 $\delta^{18}O$ and $\delta^{13}C$ records showed clear annual cycles, with $\delta^{18}O$ values varying from −8.87‰ to −5.67‰ and $\delta^{13}C$ values from −9.46‰ to −6.13‰ (Figure 3). Our previous study shows a good replication of the $\delta^{18}O$ and $\delta^{13}C$ records from E'mei and Yongquan caves, suggesting EM1 is less influenced by the kinetic fractionation during the growth (Zhang et al., 2018). Variations of growth rate caused changes in lamina thickness, resulting in different resolutions of EM1 $\delta^{18}O$ and $\delta^{13}C$ records at different time periods. For example, between 1951 and 1991 AD, $\delta^{18}O$ and $\delta^{13}C$ records exhibited distinct seasonal cycles. Between 1928 and 1950 AD, $\delta^{18}O$ and $\delta^{13}C$ records consisted of seasonal cycles and annual cycles. On the long-term scale, the $\delta^{18}O$ values exhibited more positive trends during 1928–1950 and 1977–1991 AD than in the interval of 1951–1976 AD (Figure 3), which might be related to the stronger monsoon intensity in 1951–1976 AD (Zhang et al., 2018). Previous studies based on instrumental data show a strong-to-weak shift of the summer monsoon intensity from 1951–1976 AD to 1977–1991 AD (Gong and Ho, 2002; Zhou et al., 2009).

The seasonal amplitude of EM1 $\delta^{13}C$ was smaller than that of $\delta^{18}O$. The EM1 $\delta^{18}O$ and $\delta^{13}C$ records showed an offset of ~4 months in most years except for a few years (1965, 1971, 1983) that were in phase. $\delta^{13}C$ values were lower in WPSL and higher in TDSL (Figure 3). The oscillation of $\delta^{18}O$ exhibited clear seasonal characteristics, and $\delta^{18}O$ showed the minimum or minimum to maximum values in TDSL. The annual seasonal variation of EM1 $\delta^{18}O$ is basically consistent with that of precipitation $\delta^{18}O$ from the GNIP Changsha station during 1988–1991 AD and IsoGSM simulated precipitation $\delta^{18}O$ during 1979–1991 AD, showing a positive correlation with simulated precipitation $\delta^{18}O$ [r=0.453; 95% confidence interval (0.31; 0.575)] (Figure 4). Lower $\delta^{18}O$ values were observed during July-September and higher values during December-April. According to the water-calcite fractionation Equation 1,

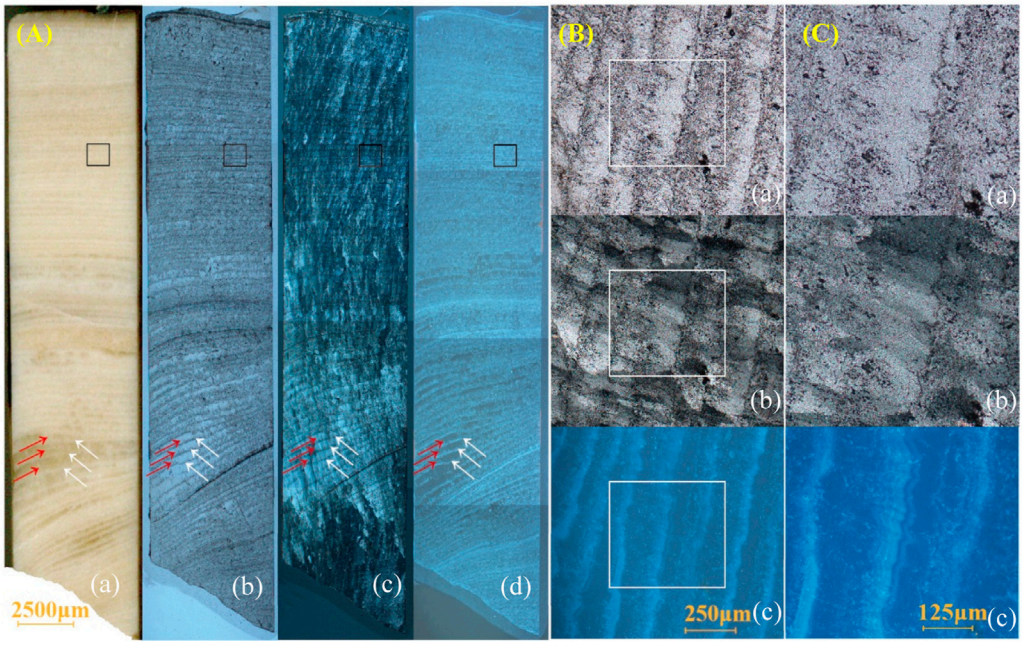

FIGURE 2
Lamina characteristics of stalagmite EM1. **(A)** (a) profile of EM1; (b–d): images of layers with very clear growth laminae under (b) transmitted light, (c) cross-polarized light and (d) blue-light epifluorescence. DTSL (red arrows) corresponds to the light transmittance layer under transmitted light, and the non-luminescent layer under fluorescence; WPSL (white arrows) corresponds to the opaque layer under transmitted light and the weak to strong luminescence band under fluorescence. **(B)** magnified images of the black rectangle in **(A)**, where **(C)** is the amplified region of the white rectangle in **(B)**; the fluorescence layer in **(C)** (c) has uniform width, and inner fluorescent sublayers are clearly visible.

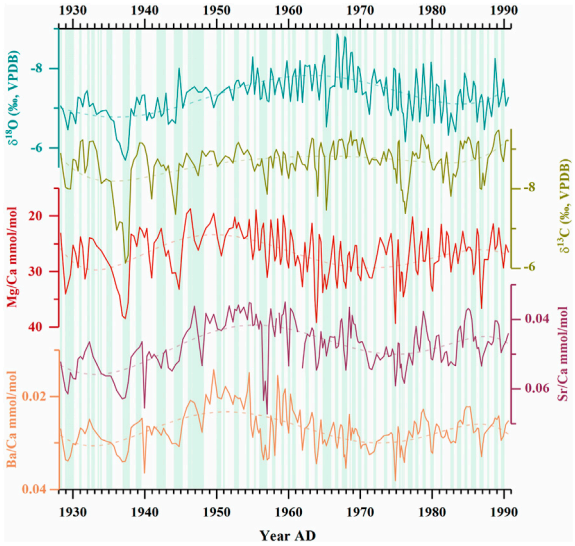

FIGURE 3
Variations of stable isotopes ($\delta^{18}O$ and $\delta^{13}C$) and trace element ratios (Mg/Ca, Sr/Ca, and Ba/Ca) in EM1 from 1928 to 1991 AD and their relationship with DTSL and WPSL sublayers. The light green (white) bars represent DTSL (WPSL).

simulated calcite $\delta^{18}O$ values were also calculated using IsoGSM simulated precipitation $\delta^{18}O$. The result showed that the seasonal variation trends of simulated calcite $\delta^{18}O$ are consistent with those of EM1 $\delta^{18}O$, but the variation range of the simulated calcite $\delta^{18}O$ was higher (−11.50 to −1.78‰, VPDB) than that of EM1 $\delta^{18}O$ (−8.25 to −6.32‰, VPDB) (Figure 4).

4.3 Trace element ratios

The seasonal and interdecadal variations of Sr/Ca were always consistent with Ba/Ca in EM1, but the relationship of Mg/Ca with Sr/Ca and Ba/Ca showed some changes at different timescales (Figure 3, Supplementary Figure S3). In the long term (1928–1991 AD), Mg/Ca, Sr/Ca and Ba/Ca showed coherent variations, exhibiting an antiphase relationship with $\delta^{18}O$ (Figure 3).

During 1951–1976 AD, seasonal Mg/Ca, Sr/Ca and Ba/Ca showed variations in phase, which are also consistent with $\delta^{13}C$. However, Mg/Ca showed an antiphase relationship with Sr/Ca and Ba/Ca in a few years, such as 1953, 1972, and 1973. The annual cycles of Mg/Ca showed an antiphase relationship with Sr/Ca and Ba/Ca in most years during 1977–1991 AD, with coherent variations between Mg/Ca, Sr/Ca, and Ba/Ca in few years (e.g., 1979, 1985–1986). Remarkably, when the seasonal variations of Mg/Ca are in phase with Sr/Ca and Ba/Ca, $\delta^{13}C$ also varies in phase with them (Supplementary Figure S3). During 1951–1991 AD, an in-phase relationship between Mg/Ca and $\delta^{13}C$ and an antiphase relationship between Mg/Ca and $\delta^{18}O$ were observed. The relationships between Mg/Ca ratios and sublayers are clearly visible, with lower Mg/Ca ratios corresponding to WPSL and higher Mg/Ca ratios within TDSL (Figure 3).

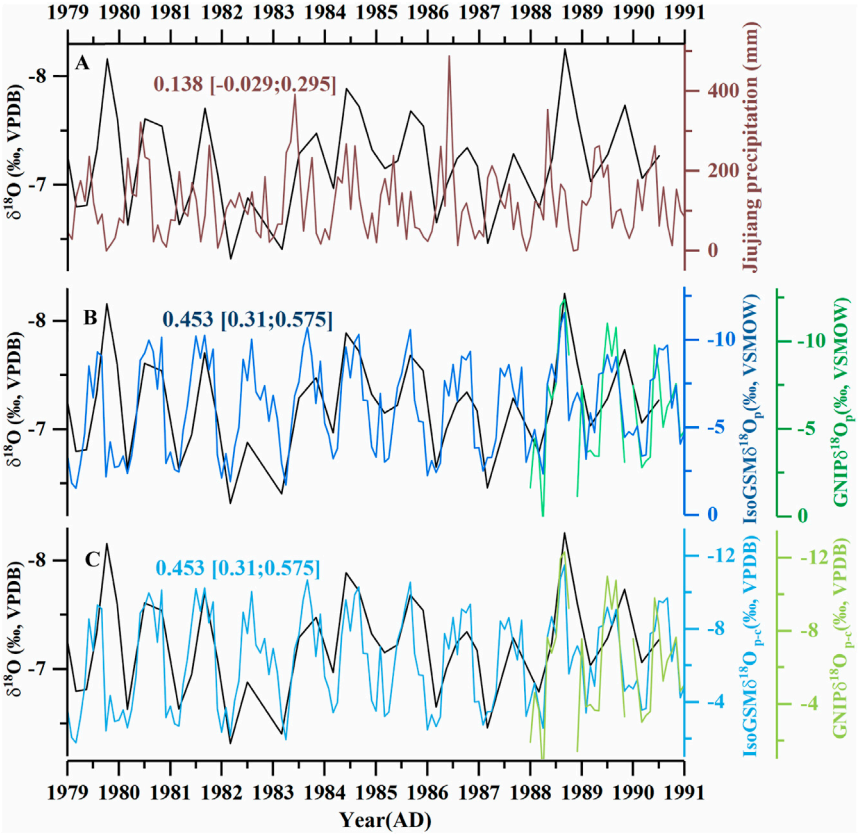

FIGURE 4
Comparison between EM1 $\delta^{18}O$, precipitation $\delta^{18}O_p$, and simulated calcite $\delta^{18}O_{p\text{-}c}$ records. **(A)** EM1 $\delta^{18}O$ (black curve) is not significantly correlated to the monthly average precipitation at Jiujiang station (brown curve) [r=0.136 with 95% confidence interval (−0.029; 0.295)]. **(B)** EM1 $\delta^{18}O$ showing coherent variation with the monthly weighted mean precipitation $\delta^{18}O_p$ from the GNIP Changsha station and the monthly simulated precipitation $\delta^{18}O_p$ from IsoGSM, with a positive correlation between EM1 $\delta^{18}O$ and simulated $\delta^{18}O_p$ from IsoGSM [r=0.453 with 95% confidence interval (0.31; 0.575)]. **(C)** Comparison between EM1 $\delta^{18}O$ and simulated calcite $\delta^{18}O_{p\text{-}c}$ records calculated from the GNIP Changsha station $\delta^{18}O_p$ and IsoGSM simulated $\delta^{18}O_p$, EM1 $\delta^{18}O$ and simulated calcite IsoGSM$\delta^{18}O_{p\text{-}c}$ records during 1979–1991 AD show a positive correlation [r=0.453 with 95% confidence interval (0.31; 0.575)].

5 Discussion

5.1 Controlling factors of multi-proxy variations on inter-decadal scales

Zhang et al. (2018) suggested that precipitation and stalagmite $\delta^{18}O$ are influenced by precipitation seasonality and the large-scale atmosphere circulation modulated by the El Nino-Southern Oscillation (ENSO) in the study area. It was suggested that stalagmite $\delta^{18}O$ is negatively correlated with the East Asian summer monsoon (EASM)/non-summer monsoon (NSM) precipitation ratio on interannual to decadal timescales because the EASM/NSM ratio are predominantly affected by ENSO (Zhang et al., 2018; Zhang et al., 2020). A good correlation was observed between EM1 $\delta^{18}O$, precipitation amount, and dry/flood (D/F) from 1970 to 1991, with lower (higher) EM1 $\delta^{18}O$ corresponding to decreased (increased) D/F index and increased (decreased) precipitation in the study area (Figure 5). From 1928 to 1970 AD, the D/F index and EM1 $\delta^{18}O$ showed weak correlation (Figure 5), which is considered to be driven by the variation of precipitation seasonality associated with shifts in oceanic-atmospheric circulation (Zhang et al., 2018). Previous studies have proved that the PDO/ENSO circulation shifted from a cold phase during 1951–1976 AD to a warm phase during 1977–1990 AD (Chan and Zhou, 2005) (Supplementary Figure S4), and different phases of ENSO or PDO have important effects on EASM precipitation in southeastern China by regulating the intensity and position of WPSH (Wang and Lin., 2002; Dong and Xue, 2016). The comparison between EM1 $\delta^{18}O$, PDO, MEI, and WPSH in this study suggest that lower (higher) $\delta^{18}O$ values correspond to a weakened (strengthened) WPSH associated with cold (warm) PDO/ENSO phases on the inter-annual to inter-decadal timescales (Supplementary Figure S4), which is a reasonable explanation for the antiphase relationship between stalagmite $\delta^{18}O$ and the EASM/NSM ratio modulated by ENSO during 1951–1991 (Figure 5).

Stalagmite $\delta^{13}C$ can be influenced by the $\delta^{13}C$ values of soil and atmospheric CO_2 (Baskaran and Krishnamurthy, 2013; Tan, 2013; Li and Liu, 2015). $\delta^{13}C$ can reflect regional vegetation controlled by hydroclimate conditions and human activities on centennial-to-millennial scales (Zhang et al., 2015; Niu et al., 2022). Over annual to decadal scales, $\delta^{13}C$ can be also largely influenced by the processes of

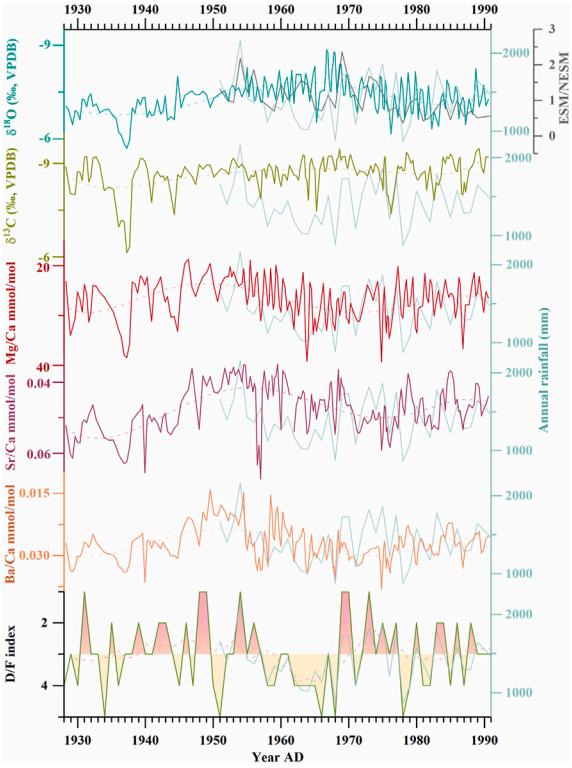

FIGURE 5
Comparison between EM1 multi-proxy records (1928–1991 AD) and annual precipitation and D/F index records of Jiujiang region. The D/F index was reconstructed from drought and flood events during spring, summer, and autumn recorded in historical literature, reflecting the local precipitation variation.

PCP in epikarst systems, degassing speed of CO_2 within caves, bedrock dissolution and residence time of seepage water (Tan, 2013). Studies demonstrated that PCP usually induces a consistent increase of $\delta^{13}C$, Mg/Ca, Sr/Ca, and Ba/Ca (Mattey et al., 2010; Sinclair et al., 2012; Koltai et al., 2017; Vansteenberge et al., 2020). The $\delta^{13}C$ values of EM1 from 1928 to 1991 did not exhibit any distinct change (Figure 5), probably due to the lack of apparent changes in the overlying vegetation in the past 70 years. EM1 $\delta^{13}C$ exhibited several inconspicuous cycles on annual to decadal scales, with a strong covariation of increased $\delta^{18}O$, Mg/Ca, Sr/Ca and Ba/Ca values, indicating the occurrence of PCP during these dry periods on annual to decadal timescales (Figure 5).

On the interdecadal scale, Mg/Ca, Sr/Ca, and Ba/Ca records showed in-phase variation, which are in antiphase with annual precipitation amount (Figure 5). The relationship between trace element ratios and the D/F index of the study area during 1928–1991 AD was also investigated, with higher (lower) Mg/Ca, Sr/Ca, and Ba/Ca ratios corresponding to dry (wet) climate (Figure 5). The response rates of Mg, Sr, and Ba to hydroclimate change were different (Mg>Ba>Sr) (Figure 5), which might be attributable to the different distribution coefficients of these trace elements (Mg<<Ba<Sr) (Fairchild and Baker, 2012; Day and Henderson, 2013). This indicates that Mg is more sensitive to precipitation variations than Ba and Sr. On interdecadal timescales, with decreased precipitation, the extended residence time of seepage water in the epikarst system enhances WRI, which is conducive to the dissolution of Mg, Sr, and Ba in bedrock and finally lead to higher Mg/Ca, Sr/Ca, and Ba/Ca ratios. The fact that higher values of Sr/Ca and Ba/Ca corresponded to increased rainfall from 1972 to 1976 AD indicate that the incorporation of Sr and Ba into speleothem might have a more complex mechanism (Figure 5). On the interdecadal scale, Mg/Ca, Sr/Ca, and Ba/Ca in EM1 were found to respond to local hydroclimate conditions, with higher values in dry climates.

5.2 Controls on the seasonal variability of $\delta^{18}O$ and $\delta^{13}C$

Several studies have determined the seasonal variation of stalagmite $\delta^{18}O$ through modern analysis techniques to explore the relationship between sub-annual climatic and cave environmental signals (Johnson et al., 2006; Baker et al., 2007; Orland et al., 2009; Orland et al., 2012; Koltai et al., 2017; Baker et al., 2019). Figure 4 and Figure 6 show a clear seasonal cycle of EM1 $\delta^{18}O$, EM1 retains seasonal climate responses probably because of abundant rainfall and the suitable cave environment. A comparison between EM1 $\delta^{18}O$ records and meteorological data reveals that the seasonal variation of EM1 $\delta^{18}O$ is significantly and positively correlated with precipitation $\delta^{18}O$ but insignificantly correlation with precipitation amount (Figure 4). Cave monitoring studies from Shennong cave (around 200 km southeast of E'mei cave) and the study area show that there is more rainfall in spring with more positive $\delta^{18}O$ values but less rainfall in summer with more negative $\delta^{18}O$ values, this is not consistent with "amount effect" (Zhang et al., 2020; Tian et al., 2021). The relationship between seasonal rainfall amount and rainfall $\delta^{18}O$ is consistent with that between seasonal rainfall amount and speleothem $\delta^{18}O$ (Figure 1 and Figure 4). Therefore, we suggest that the "amount effect" does not fit the speleothem $\delta^{18}O$ values in southeastern China on seasonal timescales.

We also find that the seasonal variation range $\delta^{18}O$ in EM1 (−8.25 ~ −6.32‰, VPDB) was much smaller compared to the simulated calcite $\delta^{18}O$ (−11.50 ~ −1.78‰, VPDB) (Figure 4). Some potential mechanisms can blur or alter seasonal $\delta^{18}O$ signals from precipitation to stalagmites, such as selective recharging (Baker et al., 2007; Baker et al., 2019), mixing of old and fresh water (Baker et al., 2007; Baker and Bradley, 2010), seepage path (Duan et al., 2016; Markowska et al., 2016), and evaporative fractionation in the soil and epikarst zone (Zimmerman et al., 1967). Cai et al. (2010) found that $\delta^{18}O$ in stalagmites from northwestern Thailand and 5-year moving average of the local rainfall data has a better correlation than that comparing with 1-year moving average of the rainfall data, indicating a retention and mixing of old and fresh water in karst system. On the basis of the correlation analysis between stalagmite $\delta^{18}O$ and precipitation, Jex et al. (2010) concluded that the drip water is supplied by an aquifer recharged by waters from the current year and the previous 5 years. Regression correlation between original monthly rainfall and EM1 $\delta^{18}O$ [r=0.453; 95% confidence interval (0.31; 0.575)] is worse than the correlation between 8-point smoothed rainfall data and EM1 $\delta^{18}O$

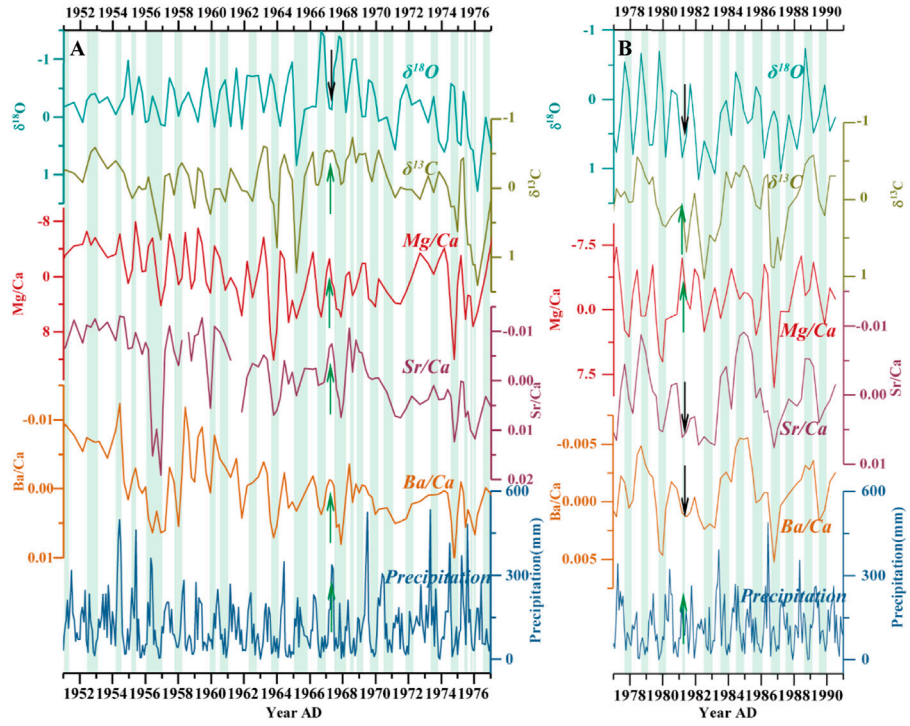

FIGURE 6
Comparison between EM1 multi-index records (1951–1991 AD, detrended) and meteorological data from Jiujiang station (1951–1991 AD), with the light green bar indicating TDSL. **(A)**: Strong monsoon period (1951–1976 AD). $\delta^{13}C$ showing in-phase relationships with Mg/Ca, Sr/Ca, and Ba/Ca with high values (low values) corresponding to the dry (wet) season, and $\delta^{18}O$ showing antiphase relationships with $\delta^{13}C$, Mg/Ca, Sr/Ca, and Ba/Ca in the detrended data. **(B)**: Weak monsoon period (1977–1991 AD). $\delta^{18}O$ and Mg/Ca cycles showing inverse changes, and $\delta^{18}O$ showing in-phase relationships with Sr/Ca and Ba/Ca. High Mg/Ca values (low Sr/Ca and Ba/Ca values) correspond to the dry season (light green bar indicates DTSL).

[r=0.486; 95% confidence interval (0.348; 0.603)], which indicates a mixing of old and fresh water in the epikarst (Baker and Bradley, 2010). When the temperature is high, precipitation may have undergone evaporation in soil or near surface water during the formation of EM1 drips, resulting in heavier $\delta^{18}O$ values of the drip water than the original precipitation $\delta^{18}O$ (Baker et al., 2007; Markowska et al., 2016). Our monitoring work in Shennong cave also shows that the $\delta^{18}O$ values of drip water inside the cave are significantly higher than the $\delta^{18}O$ values of original precipitation, and the amplitude of drip water $\delta^{18}O$ is smaller than original precipitation (Tian et al., 2021), indicating evaporation occurs in the process from precipitation to drip water. Unfortunately, monitoring work was not performed in the E'mei cave. However, we can find the most negative values of simulated calcite $\delta^{18}O$ (−11.50‰, VPDB) are lower than those of the EM1 $\delta^{18}O$ (−8.25‰, VPDB) during summer when the precipitation $\delta^{18}O$ is negative but the temperature is high (Figure 4). The amplitude of simulated calcite $\delta^{18}O$ (~9.72‰, VPDB) is much larger than that of EM1 $\delta^{18}O$ (~1.93‰, VPDB). These observations indicate that evaporation and water mixing occur in the process from the precipitation, drip water to speleothem in the E'mei cave.

Seasonal $\delta^{18}O$ in EM1 peaks in spring (March-May) with high rainfall, decreases with the onset of the summer monsoon, and reaches the lowest level in late summer to early autumn with significantly reduced rainfall and strong evaporation. The high EM1 $\delta^{18}O$ values in WPSL (luminescent layer) correspond to a large amount of precipitation with higher $\delta^{18}O$ in the spring to early summer (Figure 6). The low EM1 $\delta^{18}O$ values in TDSL (non-luminescent layer) are consistent with the low precipitation $\delta^{18}O$ occurring during the late summer to early autumn when stalagmite sublayers are deficient in organic matter due to less precipitation and strong evaporation (low P-E), which are not conducive to soil organic matter production (Davidson et al., 2000; Fischer, 2009; Wang et al., 2016) and eluviation (Beynen et al., 2002). This further confirms the hypothesis of the seasonal variation of precipitation $\delta^{18}O$ primarily controlling the seasonal variation of EM1 $\delta^{18}O$.

The seasonal variation of $\delta^{13}C$ in cave sediments may be affected by various processes, such as bedrock dissolution (Riechelmann et al., 2011), soil biogenic CO_2 content (Fairchild et al., 2006), degassing of CO_2 (Sinclair et al., 2012), and PCP (Rampelbergh et al., 2014a). Seasonal cycles of $\delta^{13}C$ are much less pronounced than those of $\delta^{18}O$, but an inverse correlation between seasonal $\delta^{18}O$ and $\delta^{13}C$ records could still be observed, with the minima of $\delta^{13}C$ corresponding to the maxima (or maxima to minima) of $\delta^{18}O$ (March-June) and the maxima of $\delta^{13}C$ corresponding to the minima (or minima to maxima) of $\delta^{18}O$ (July-February) (Figure 6). These can be attributed to the continuous spring precipitation from March to May and June being the Meiyu period in the region. In addition, the average temperature from March to June is suitable for plant growth. Therefore, soil contains more CO_2 rich in ^{12}C because of flourishing plant roots and strong soil microbial activity (Amundson et al., 1998; Zhang et al., 2015). At

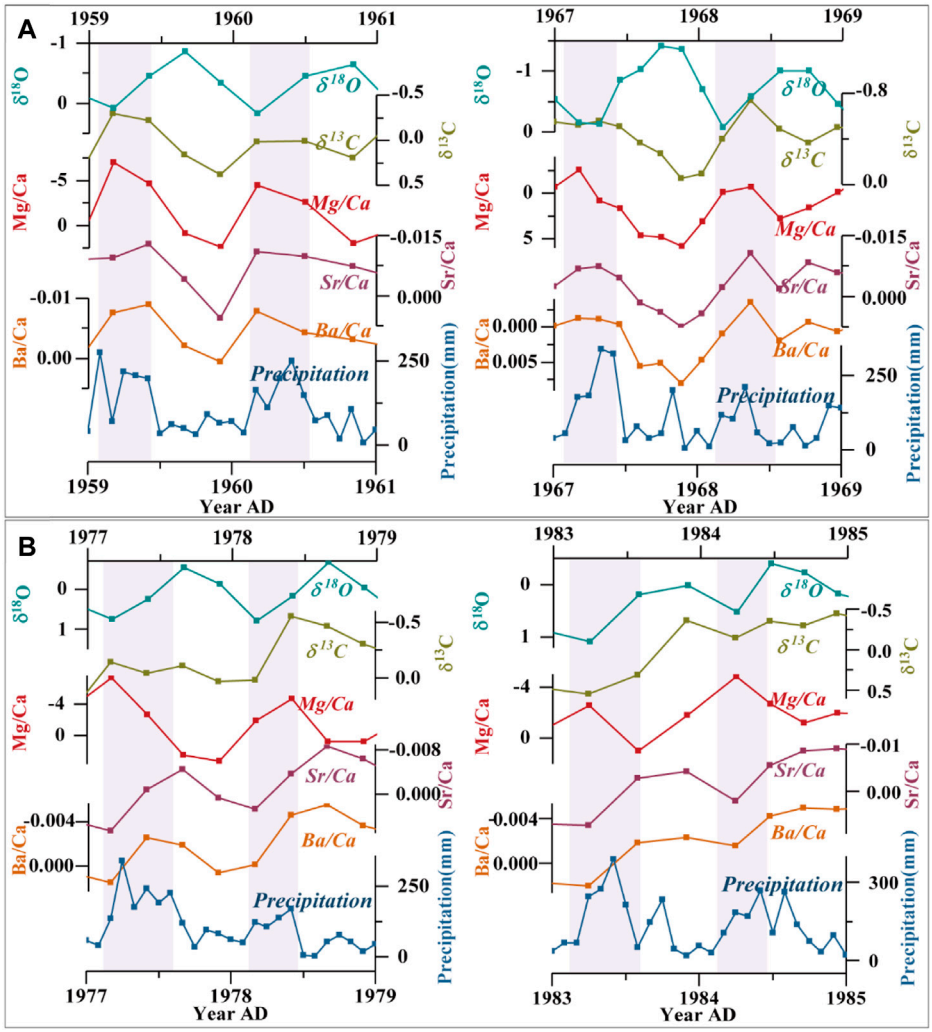

FIGURE 7
Local enlarged images of the strong monsoon period **(A)** and the weak monsoon period **(B)** in Figure.6 (mauve bar describes the wet season).

the same time, the $\delta^{13}C$ values of calcite tend to be lower because the faster drip rates are not conducive to CO_2 degassing (Banner et al., 2007; Fairchild et al., 2006). Rapid degassing of CO_2, which is mainly controlled by good ventilation or slow drip rate, leads to increases in calcite $\delta^{13}C$ (Duan et al., 2013; Johnson et al., 2006). From July to August, the decrease of rainfall and the increase of temperature in this area not only contributed to the dissolution of cave bedrock (Asrat et al., 2018), but also weakened the activities of plant roots and soil microorganisms because of low P-E, and slower drip rates promoted CO_2 degassing (Banner et al., 2007). It is noteworthy that $\delta^{13}C$ and $\delta^{18}O$ displayed similar seasonal trends in individual years (e.g., 1965, 1971, 1983–1984). The $\delta^{18}O$, $\delta^{13}C$, Mg/Ca, Sr/Ca, Ba/Ca, of EM1 in the spring of 1965 and 1971 all showed high values. This may be attributable to piston flow. During the period of heavy spring rain, resident water in the surface karst in winter was flushed out, which may have been affected by PCP (Arbel et al., 2010). From 1983 to 1984, $\delta^{18}O$ and $\delta^{13}C$ showed in phase variation but antiphase variation with Mg/Ca, Sr/Ca, and Ba/Ca (Figure 7B), and the variation ranges of $\delta^{13}C$ were 0.083‰ and 0.20‰, respectively (Figure 5). Therefore, rather than PCP, bedrock dissolution is suggested to be the cause of the $\delta^{13}C$ increase under this scenario (Riechelmann et al., 2011).

5.3 Controls on the seasonal change cycle of trace-elements

5.3.1 Strong monsoon period (1951–1976 AD)

On a seasonal scale, a strong covariation of Mg/Ca with Sr/Ca and Ba/Ca and $\delta^{13}C$ was found during 1951–1976, and they were in antiphase with seasonal $\delta^{18}O$ variation. Higher (lower) values of Mg/Ca, Sr/Ca, and Ba/Ca were observed in TDSL (WPSL), corresponding to the dry (wet) season (Figure 6A). Figure 7A displays more distinct relationships between them in detail. These relationships have generally been considered to reflect a PCP in the epikarst zone during a dry period (Fairchild et al., 2000; Johnson et al., 2006; Rampelbergh et al., 2014b; Riechelmann et al., 2020). In addition, studies have suggested that the preferential

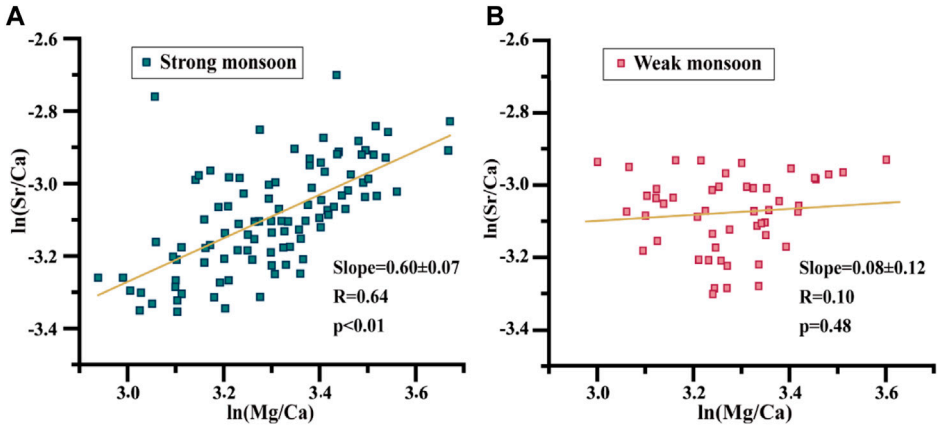

FIGURE 8
ln (Mg/Ca) vs. ln (Sr/Ca) in EM1 during the strong monsoon period **(A)** (1951–1976 AD, green) and the weak monsoon period **(B)** (1977–1991 AD, red).

dissolution of Mg, Sr, and Ba relative to Ca^{2+} may lead to increased X/Ca values in drip water and stalagmite during ICD (McGillen and Fairchild, 2005; Casteel and Banner, 2015). Using a model based on a stable karst environment, Sinclair (2010) realized that the boosted partial dissolution of limestone will result in the higher enrichment of Mg/Ca and Sr/Ca in stalagmite than host rock because of ICD. Typically, enhanced WRI (including the incongruent dissolution of dolomite or dolomite/calcite recrystallization) during a dry period may also lead to increased Mg/Ca and Sr/Ca in stalagmite (Tan et al., 2015) because of increased bedrock dissolution (Baldini et al., 2002; Musgrove and Banner, 2004). Through mathematical modeling, Sinclair (2010), Sinclair et al. (2012) predicted that PCP/ICD will lead to a linear correlation with a theoretical slope (0.88± 0.13) in graphs of ln (Sr/Ca) vs. ln (Mg/Ca) independent of host rock or dripwater composition. The combined process of WRI and PCP/ICD is indicated by slopes below 0.709, with lower slope implying stronger WRI (Casteel and Banner, 2015; Zhang et al., 2019). In this study, the slopes of ln (Mg/Ca) vs. ln (Sr/Ca) during the strong monsoon period (1951–1976 AD) was 0.60 ± 0.07 (Figure 8A). Accordingly, the seasonal variation of Mg/Ca, Sr/Ca and Ba/Ca in the strong monsoon period (1951–1976 AD) may be dominated by the combined effect of WRI and PCP/ICD, which leads to the increase of trace element ratios during dry periods (late summer to winter) and decrease in the wet periods (spring and early summer) because of the dilution effect of recharge water (Gascoyne, 1983; Baldini et al., 2006; Tadros et al., 2016; Tadros et al., 2019).

5.3.2 Weak monsoon period (1977–1991 AD)

The seasonal cycles of Mg/Ca, and Sr/Ca, Ba/Ca transformed to dominantly antiphase during the weak monsoon period (1977–1991 AD) (Figure 6B, Figure 7B). Zhang et al. (2018) found the annual precipitation changed little between La Niña and El Niño years, but the precipitation seasonality (summer monsoon *versus* non-summer-monsoon precipitation amount) significantly change in the study area. During the weak monsoon period, the relatively increased precipitation in late summer-autumn (Supplementary Figure S5) was not conducive to the occurrence of PCP and ICD and weakened the controls of PCP/ICD and WRI on Sr/Ca and Ba/Ca. Although the slopes of ln (Mg/Ca) *versus* ln (Sr/Ca) in EM1 from 1977 to 1991 was 0.08 ± 0.12 (Figure 8B) and WRI may promote incongruent dissolution of dolomite (IDD of $CaMg(CO_3)_2$) to produce an antiphase relationship with Mg/Ca, Sr/Ca, and Ba/Ca (Roberts et al., 1998; Baldini et al., 2006), ln (Mg/Ca) and ln (Sr/Ca) did not show any correlation (Figure 8B) and the effect of IDD was limited by the dolomite content in the bedrock (Fairchild and Treble, 2009) or/and the residence time of retained water (Fairchild et al., 2006). The water recharge time in autumn during the strong monsoon period (1951–1977 AD) was significantly longer than during the weak monsoon period (1977–1991 AD) (Supplementary Figure S5), but no influence of IDD on the variation of trace element ratios in EM1 was observed during the strong monsoon period (1951–1976 AD) (Figure 6A). Therefore, it is not suggested that WRI account for the inverse changes of Mg/Ca and Sr/Ca, Ba/Ca during periods of weak monsoon.

Experimental studies and stalagmite data have indicated an increase in Sr and Ba with higher growth rates (Huang and Fairchild, 2001; Treble et al., 2003; Mcmillan et al., 2005; Johnson et al., 2006; Fairchild and Baker, 2012; Tan et al., 2014a). More precipitation and increased CO_2 production by soil microbial communities and tree root respiration in spring-early summer can promote bedrock dissolution to increase calcite supersaturation, which is conducive to the growth of calcite (Boch et al., 2011; Baker et al., 2021). In addition, Mg^{2+} can also retard crystal growth (Davis et al., 2000; Kim et al., 2007). The lower Mg content in spring-early summer can compensate for the decreased calcite growth, but the opposite in autumn and winter. It could be deduced that Sr and Ba may have been controlled by the seasonal variations in the growth rates of EM1 during the weak monsoon period (Mcmillan et al., 2005; Johnson et al., 2006; Fairchild and Baker, 2012; Tan et al., 2014b). The higher growth rates of EM1 in spring-early summer increases defect sites and interstitials in the calcite crystal lattice and these sites are preferentially occupied by relatively large Sr and Ba ions (Reeder and Rakovan, 1999). Correspondingly, the lower growth rates in late summer-autumn and winter may reduce the Sr and Ba content in EM1. We can find the controlling factors of seasonal Sr/Ca and Ba/Ca may vary under strong and weak monsoon conditions, which need more studies in the future by detailed cave monitoring work.

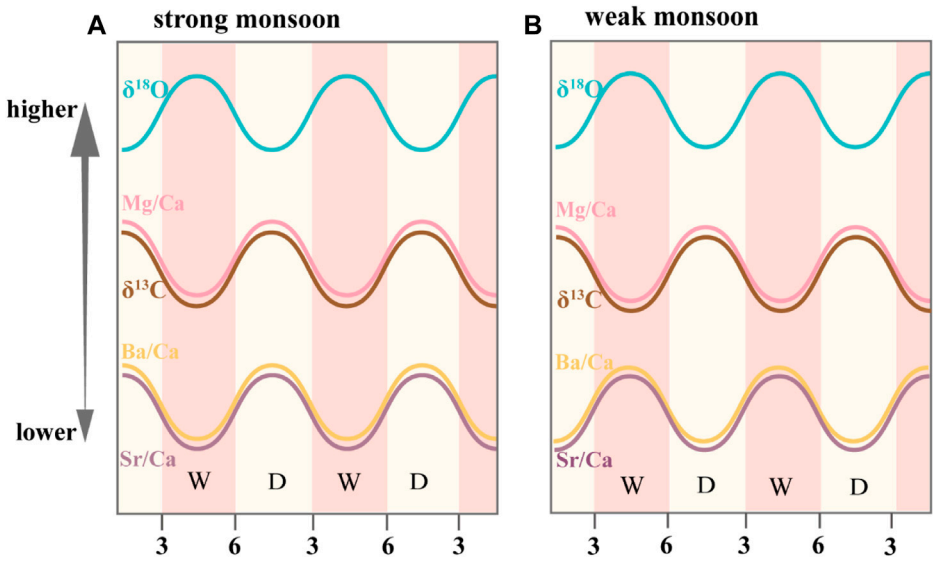

FIGURE 9
Conceptual model of content variation and correspondence of $\delta^{18}O$ (blue curves), $\delta^{13}C$ (brown curves), Mg/Ca (pink curves), Sr/Ca (purple curves), and Ba/Ca (orange curves) in the wet season (W, pink rectangle) and dry season (D, yellow rectangle) in the strong monsoon period **(A)** and weak monsoon period **(B)** (3 represents March, and 6 represents June).

5.3.3 Potential of Mg/Ca proxy in seasonal palaeohydrology studies

The high-positive correlation between Sr and Ba within both intervals (the strong and weak monsoon periods) suggests that Sr and Ba are dominated by common environmental parameters, which can be further attributed to the similar partition coefficients, ionic radii, and valence states of Sr and Ba (Desmarchelier et al., 2006; Day and Henderson, 2013). The climate influence mechanism of Sr and Ba varied under different monsoon intensities. The seasonal variations of Sr/Ca and Ba/Ca were mainly influenced by PCP/ICD and WRI with lower (higher) ratios occurring in the wet (dry) season during the strong monsoon period (Figure 9A) and controlled by growth rates with lower (higher) ratios occurring in the dry (wet) season during the weak monsoon period (Figure 9B). The seasonal cycles of Mg/Ca and $\delta^{18}O$ in EM1 remained consistently antiphase, and the peak in Mg/Ca corresponded to the minimum value or minimum to maximum of $\delta^{18}O$. A comparison between Mg/Ca and modern instrumental records revealed that the Mg/Ca ratios were the highest during late summer to winter with reduced precipitation (precipitation $\delta^{18}O$ was more negative) and the lowest during spring-early summer with increased precipitation (precipitation $\delta^{18}O$ was more positive) (Figure 1, Figure 6, Figure 9), which is consistent with the correspondence relationships between Mg/Ca, $\delta^{18}O$ and sublayer features (Zhang et al., 2022).

On the whole, higher Mg/Ca (lower $\delta^{18}O$, higher $\delta^{13}C$) corresponds to TDSL with less organic matter (non-luminescent layer), while lower Mg/Ca (higher $\delta^{18}O$, lower $\delta^{13}C$) occurs in WPSL with more organic matter (weakly to strongly luminescent layer) (Figure 6, Figure 9). Rainfall is abundant during spring-early summer such that $\delta^{18}O$ is more positive and Mg is lower in stalagmite, compared to the late summer -winter season. Moreover, from spring to early summer, the temperature and rainfall showed an increasing trend, which enhanced microbial activity in the soil of the overlying cave (Tegen and Dörr, 1996) and the increasing concentrated heavy rainfall could also effectively leach organic matter (Scott et al., 1998; Baker et al., 2008; Ban et al., 2008; Fairchild and Baker, 2012) to form WPSL with lower $\delta^{13}C$ (weak to strong luminescence band under fluorescence). Multiple extremely thin fluorescent sublayers have been observed inside several wider fluorescent layers, which may correspond to several pulses of organic matter deposition driven by multiple strong rainfall events (Figure 2C). The seasonal cycles of Mg/Ca are suggested to respond to changes in local hydrological conditions (humidity and drought), even on a seasonal scale, leading to a decrease in Mg/Ca with increased precipitation and increase with decreased precipitation.

6 Conclusion

This study presents seasonal variations of trace-elements (Mg/Ca, Sr/Ca, and Ba/Ca) and stable-isotope compositions ($\delta^{18}O$ and $\delta^{13}C$) during the period of 1928–1991 AD from an annually laminated stalagmite (EM1) in E'Mei Cave, northern Jiangxi Province, China. By comparing these index records with instrumental observation data, seasonal variations of the isotopes and trace elements in modern stalagmite EM1 and their controlling factors were emphatically discussed. The following conclusions can be drawn from the results.

(1) The annual laminae of EM1 comprise couplets of alternating TDSL (non-luminescent layer with lower $\delta^{18}O$ and higher Mg/Ca) and WPSL (weakly to strongly luminescent layer with higher$\delta^{18}O$ and lower Mg/Ca). The formation of WPSL might be attributable to a gradual increase in organic matter

under the influence of progressively enhanced soil microbial activity and eluviation during the wet season from spring to early summer. Correspondingly, TDSL formed in the dry season from late summer to winter.

(2) On the interannual and interdecadal timescales, the variations in $\delta^{18}O$ are suggested to be strongly correlated with the EASM/NSM ratio and the large-scale circulation associated with the ENSO phases. EM1 $\delta^{13}C$ is mainly influenced by vegetation overlying the cave and PCP on interannual-decadal timescales. Mg/Ca, Sr/Ca, and Ba/Ca mainly respond to local hydrological conditions on interdecadal timescales, with lower (higher) values corresponding to wet (dry) periods.

(3) The seasonal variation of the $\delta^{18}O$ signal of local precipitation is preserved in EM1, but the amplitude of changes in EM1 $\delta^{18}O$ is much smaller than that of simulated calcite $\delta^{18}O$, which might be attributable to the mixing of waters and evaporation in the epikarst system. Seasonal $\delta^{13}C$ values in EM1 are usually lower in spring and early summer and higher in autumn and winter, which is mainly affected by the soil microbial CO_2 content, with a certain contribution of PCP. The seasonal variation of Mg/Ca in EM1 consistently showed a hydrological response to rainfall input; Mg/Ca decreased with increased rainfall in spring and early summer and increased in late summer to winter with decreased rainfall. However, the controlling factors (such as PCP/ICD, WRI and growth rate) of seasonal Sr/Ca and Ba/Ca may vary under different hydrothermal conditions, which still need further exploration in the future. Mg/Ca in stalagmites has potential as an indicator of local seasonal hydrological changes. The method integrating the analysis of Mg/Ca and other multi-proxy records ($\delta^{18}O$, $\delta^{13}C$, Sr/Ca, Ba/Ca, etc.) may contribute to the reconstruction of precipitation changes on both seasonal and interannual timescales under different hydroclimate backgrounds in subtropical regions.

Data availability statement

The raw data supporting the conclusions of this article will be made available by the authors, without undue reservation.

Author contributions

HZ and YB conceived and designed the project. YB performed the experiments, interpreted the data, and wrote the manuscript. HZ revised the manuscript. YB, HZ, BM, XN, JL, and RZ contributed to data analysis and discussion. All authors contributed to the article and approved the submitted version.

Funding

This study was supported by grants from the National Science Foundation of China (NSFC: 41972186 and 41888101), the Strategic Priority Research Program of the Chinese Academy of Sciences (XDB40000000), NSFC (41703007), Project for the "Young Talent Support Plan" of Xi'an Jiaotong University, and the China Postdoctoral Science Foundation (2019T120894 and 2015M580832).

Acknowledgments

We thank Jingjie ZANG from the Institute of Earth Environment, Chinese Academy of Sciences for their generous help in the preparation and testing of trace elements.

Conflict of interest

The authors declare that the research was conducted in the absence of any commercial or financial relationships that could be construed as a potential conflict of interest.

Publisher's note

Supplementary material

The Supplementary Material for this article can be found online at: https://www.frontiersin.org/articles/10.3389/feart.2023.1135901/full#supplementary-material

References

Amundson, R., Stern, L., Baisden, T., and Wang, Y. (1998). The isotopic composition of soil and soil-respired CO2. *Geoderma* 82 (1), 83–114. doi:10.1016/s0016-7061(97)00098-0

Arbel, Y., Greenbaum, N., Lange, J., and Inbar, M. (2010). Infiltration processes and flow rates in developed karst vadose zone using tracers in cave drips. *Earth Surf. Proc. Land.* 35, 1682–1693. doi:10.1002/esp.2010

Asrat, A., Baker, A., Leng, M. J., Hellstrom, J., Mariethoz, G., Boomer, I., et al. (2018). Paleoclimate change in Ethiopia around the last interglacial derived from annually-resolved stalagmite evidence. *Quat. Sci. Rev.* 202, 197–210. doi:10.1016/j.quascirev.2018.06.016

Baker, A., and Bradley, C. (2010). Modern stalagmite $\delta^{18}O$: Instrumental calibration and forward modelling. *Glob. Planet. Change.* 71, 201–206. doi:10.1016/j.gloplacha.2009.05.002

Baker, A., Asrat, A., Fairchild, I. J., Leng, M. J., Wynn, P. M., Bryant, C., et al. (2007). Analysis of the climate signal contained within $\delta^{18}O$ and growth rate parameters in two Ethiopian stalagmites. *Geochim. Cosmochim. Ac.* 71, 2975–2988. doi:10.1016/j.gca.2007.03.029

Baker, A., Smith, C. L., Jex, C., Fairchild, I. J., and Fuller, L. (2008). Annually laminated speleothems: A review. *Int. J. Speleology Int. J Speleol. (Edizione Italiana).* 37, 193–206. doi:10.5038/1827-806X.37.3.4

Baker, A, C., Hellstrom, J., Kelly, B, F, J., Mariethoz, G., and Trouet, V. (2015). A composite annual-resolution stalagmite record of north atlantic climate over the last three millennia. *Sci. Rep.* 5, 10307. doi:10.1038/srep10307

Baker, A., Hartmann, A., Duan, W., Hankin, A., Comas-Bru, L., Cuthbert, M., O., et al. (2019). Global analysis reveals climatic controls on the oxygen isotope composition of cave drip water. *Nat. Commun.* 10, 2984. doi:10.1038/s41467-019-11027-w

Baker, A., Mariethoz, G., Comas-Bru, L., Hartmann, A., Frisia, S., Borsato, A., et al. (2021). The properties of annually laminated stalagmites-A global synthesis. *Rev. Geophy.* 59, 2. doi:10.1029/2020rg000722

Baldini, J. U., McDermott, F., and Fairchild, I. J. (2002). Structure of the 8200-year cold event revealed by a speleothem trace element record. *Science* 296, 2203–2206. doi:10.1126/SCIENCE.1071776

Baldini, J., Mcdermott, F., Baker, A., Baldini, L. M., Mattey, D. P., and Railsback, L. B. (2005). Biomass effects on stalagmite growth and isotope ratios: A 20th century analogue from wiltshire, england. *Earth Planet. Sci. Lett.* 240, 486–494. doi:10.1016/j.epsl.2005.09.022

Baldini, J., Mcdermott, F., and Fairchild, I. J. (2006). Spatial variability in cave drip water hydrochemistry: Implications for stalagmite paleoclimate records. *Chem. Geol.* 235, 390–404. doi:10.1016/j.chemgeo.2006.08.005

Baldini, J., Mcdermott, F., Baldini, L. M., Ottley, C. J., Linge, K. L., Clipson, N., et al. (2012). Identifying short-term and seasonal trends in cave drip water trace element concentrations based on a daily-scale automatically collected drip water dataset. *Chem. Geol.* 330, 1–16. doi:10.1016/j.chemgeo.2012.08.009

Ban, F., Pan, G., Zhu, J., Cai, B., and Tan, M. (2008). Temporal and spatial variations in the discharge and dissolved organic carbon of drip waters in beijing shihua cave, China. *Hydro. Process* 22, 3749–3758. doi:10.1002/hyp.6979

Ban, F., Baker, A., Marjo, C., Han, J., Duan, W., Li, X., et al. (2018). An optimized chronology for a stalagmite using seasonal trace element cycles from Shihua Cave, Beijing, North China. *Sci. Rep.* 8, 4551. doi:10.1038/s41598-018-22839-z

Banner, J. L., Guilfoyle, A., James, E. W., Stern, L. A., and Musgrove, M. L. (2007). Seasonal Variations in Modern Speleothem Calcite Growth in Central Texas, U.S.A. *J. Sediment. Res.* 77, 615–622. doi:10.2110/jsr.2007.065

Baskaran, M., and Krishnamurthy, R. V. (2013). Speleothems as proxy for the carbon isotope composition of atmospheric CO_2. *Geophy. Res. Lett.* 20, 2905–2908. doi:10.1029/93GL02690

Beynen, P. V., Schwarcz, H. P., Ford, D. C., and Timmins, G. T. (2002). Organic substances in cave drip waters: studies from Marengo Cave, Indiana. *Can. J. Earth Sci.* 39, 279–284. doi:10.1139/e01-072

Boch, R., SpöTl, C., and Frisia, S. (2011). Origin and palaeoenvironmental significance of lamination in stalagmites from katerloch cave, Austria. *Sediment* 58, 508–531. doi:10.1111/j.1365-3091.2010.01173.x

Cai, B., Pumijumnong, N., Tan, M., Muangsong, C., Kong, X., Jiang, X., et al. (2010). Effects of intraseasonal variation of summer monsoon rainfall on stable isotope and growth rate of a stalagmite from northwestern Thailand. *J. Geophys. Res.* 115, D21104. doi:10.1029/2009jd013378

Casteel, R. C., and Banner, J. L. (2015). Temperature-driven seasonal calcite growth and drip water trace element variations in a well-ventilated Texas cave: Implications for speleothem paleoclimate studies. *Chem. Geol.* 392, 43–58. doi:10.1016/j.chemgeo.2014.11.002

Chan, J. C., and Zhou, W. (2005). PDO, ENSO and the early summer monsoon rainfall over south China. *Geophy. Res. Lett.* 32, L08810. doi:10.1029/2004GL022015

Cruz, F. W., Burns, S. J., Jercinovic, M., Karmann, I., and Vuille, M. (2007). Evidence of rainfall variations in southern Brazil from trace element ratios (Mg/Ca and Sr/Ca) in a late pleistocene stalagmite. *Geochim. Cosmochim. Ac.* 71, 2250–2263. doi:10.1016/j.gca.2007.02.005

Davidson, E. A., Verchot, L. V., Cattanio, J. H., Ackerman, I. L., and Carvalho, J. E. M. (2000). Effects of soil water content on soil respiration in forests and cattle pastures of eastern amazonia. *Biogeochem* 48, 53–69. doi:10.1023/a:1006204113917

Davis, K. J., Dove, P. M., and De Yoreo, J. J. (2000). The role of Mg^{2+} as an impurity in calcite growth. *Science* 290, 1134–1137. doi:10.1126/science.290.5494.1134

Day, C. C., and Henderson, G. M. (2013). Controls on trace-element partitioning in cave-analogue calcite. *Geochim. Cosmochim. Ac.* 120, 612–627. doi:10.1016/j.gca.2013.05.044

Desmarchelier, J. M., Hellstrom, J. C., and Mcculloch, M. T. (2006). Rapid trace element analysis of speleothems by ELA-ICP-MS. *Chem. Geol.* 231, 102–117. doi:10.1016/j.chemgeo.2006.01.002

Ding, Y., Liang, P., Liu, Y., and Zhang, Y. (2020). Multiscale Variability of Meiyu and Its Prediction: A New Review. *J. Geophy. Res.* 125, 7. doi:10.1029/2019JD031496

Dong, X., and Xue, F. (2016). Phase transition of the Pacific decadal oscillation and decadal variation of the East Asian summer monsoon in the 20th century. *Adv. Atmos. Sci.* 33, 330–338. doi:10.1007/s00376-015-5130-7

Duan, W., Cai, B., Tan, M., Liu, H., and Zhang, Y. (2013). The growth mechanism of the aragonitic stalagmite laminae from yunnan xianren cave, sw China revealed by cave monitoring. *Boreas* 41, 113–123. doi:10.1111/j.1502-3885.2011.00226.x

Duan, W., Ruan, J., Luo, W., Li, T., Tian, L., Zeng, G., et al. (2016). The transfer of seasonal isotopic variability between precipitation and drip water at eight caves in the monsoon regions of China. *Geochim. Cosmochim. Ac.* 183, 250–266. doi:10.1016/j.gca.2016.03.037

Fairchild, I. J., and Baker, A. (2012). *Speleothem science: From process to past environments*. Wiley. doi:10.1002/9781444361094

Fairchild, I., J., and Treble, P. C. (2009). Trace elements in speleothems as recorders of environmental change. *Quat. Sci. Rev.* 28, 449–468. doi:10.1016/j.quascirev.2008.11.007

Fairchild, I. J., Borsato, A., Tooth, A. F., Frisia, S., Spiro, B., Huang, Y., et al. (2000). Controls on trace element (Sr-Mg) compositions of carbonate cave waters: implications for speleothem climatic records. *Chem. Geol.* 166, 255–269. doi:10.1016/S0009-2541(99)00216-8

Fairchild, I. J., Smith, C. L., Baker, A., Fuller, L., Spötl, C., Mattey, D., et al. (2006). Modification and preservation of environmental signals in speleothems. *Earth-Sci. Rev.* 75, 105–153. doi:10.1016/j.earscirev.2005.08.003

Fischer, T. (2009). Substantial rewetting phenomena on soil respiration can be observed at low water availability. *Soil boil. biochem.* 41, 1577–1579. doi:10.1016/j.soilbio.2009.04.009

Francisco, W., Cruz, J., Ivo, K., Oduvaldo, V. J., Stephen, J. B., Jose´ A, F., et al. (2005). Stable isotope study of cave percolation waters in subtropical Brazil: implications for paleoclimate inferences from speleothems. *Chem. Geol.* 220, 245–262. doi:10.1016/j.chemgeo.2005.04.001

Gabitov, R. I., and Watson, E. B. (2006). Partitioning of strontium between calcite and fluid. *Geochem. Geophy. Geosy.* 7, 11. doi:10.1029/2005GC001216

Gascoyne, M. (1983). Trace-element partition coefficients in the calcite-water system and their paleoclimatic significance in cave studies. *J. Hydrol.* 61, 213–222. doi:10.1016/0022-1694(83)90249-4

Genty, D., and Quinif, Y. (1996). Annually laminated sequences in the internal structure of some Belgian stalagmites; importance for paleoclimatology. *Sediment. Res.* 66, 275–288. doi:10.1306/D426831A-2B26-11D7-8648000102C1865D

Gong, D. Y., and Ho, C. H. (2002). Shift in the summer rainfall over the Yangtze River valley in the late 1970s. *Geophy. Res. Lett.* 29, 78-1–78-4. doi:10.1029/2001GL014523

Huang, Y., and Fairchild, I. J. (2001). Partitioning of sr2+ and mg2+ into calcite under karst-analogue experimental conditions. *Geochim. Cosmochim. Ac.* 65, 47–62. doi:10.1016/S0016-7037(00)00513-5

Jex, C. N., Baker, A., Fairchild, I. J., Eastwood, W. J., Leng, M. J., Sloane, H. J., et al. (2010). Calibration of speleothem $\delta^{18}O$ with instrumental climate records from Turkey. *Glob. Planet. Change.* 71, 207–217. doi:10.1016/j.gloplacha.2009.08.004

Johnson, K. R., Hu, C., Belshaw, N. S., and Henderson, G. M. (2006). Seasonal trace-element and stable isotope variations in a Chinese speleothem: the potential for high-resolution paleomonsoon reconstruction. *Earth Planet. Sci. Lett.* 244, 394–407. doi:10.1016/j.epsl.2006.01.064

Karmann, I., Cruz, F. W., Viana, O., and Burns, S. J. (2007). Climate influence on geochemistry parameters of waters from santana–pérolas cave system, Brazil. *Chem. Geol.* 244, 232–247. doi:10.1016/j.chemgeo.2007.06.029

Kim, S. T., and O'Neil, J. R. (1997). Equilibrium and nonequilibrium oxygen isotope effects in synthetic carbonates. *Geochim. Cosmochim. Ac.* 61, 3461–3475. doi:10.1016/S0016-7037(97)00169-5

Kim, S. T., O'Neil, J. R., Hillaire-Marcel, C., and Mucci, A. (2007). Oxygen isotope fractionation between synthetic aragonite and water: influence of temperature and Mg^{2+} concentration. *Geochim. Cosmochim. Ac.* 71, 4704–4715. doi:10.1016/j.gca.2007.04.019

Koltai, G., Spötl, C., Luetscher, M., Cheng, H., Barrett, S. J., and Müller, W. (2017). The nature of annual lamination in carbonate flowstones from non-karstic fractures, Vinschgau (northern Italy). *Chem. Geol.* 457, 1–14. doi:10.1016/j.chemgeo.2017.02.019

Li, L., and Liu, Z. (2015). Research Status of Climatic Implications of Oxygen and Carbon Isotopic Compositions in Cave Drip Water-Carbonate Systems. *Earth Environt* 43, 223–232. doi:10.14050/j.cnki.1672-9250.2015.02.013

Lin, F., Tan, L., Xue, G., Cheng, X., Zhang, H., Cheng, H., et al. (2021). Seasonality of precipitation recorded in a modern (1907–2008) annually laminated stalagmite from central China. *Palaeogeogr. Palaeoclimatol. Palaeoecol.* 576, 110489. doi:10.1016/j.palaeo.2021.110489

Lu, J., Zhang, H., Li, H., Sha, L., Zhao, J., Cheng, H., et al. (2021). A 120-year seasonally resolved speleothem record of precipitation seasonality from southeastern China. *Quat. Sci. Rev.* 264, 107023. doi:10.1016/j.quascirev.2021.107023

Markowska, M., Baker, A., Andersen, M. S., Jex, C. N., Cuthbert, M. O., Rau, G. C., et al. (2016). Semi-arid zone caves: evaporation and hydrological controls on $\delta^{18}O$ drip water composition and implications for speleothem paleoclimate reconstructions. *Quat. Sci. Rev.* 131, 285–301. doi:10.1016/j.quascirev.2015.10.024

Mattey, D., Lowry, D., Duffet, J., Fisher, R., Hodge, E., and Frisia, S. (2008). A 53 year seasonally resolved oxygen and carbon isotope record from a modern gibraltar speleothem: reconstructed drip water and relationship to local precipitation. *Earth Planet. Sci. Lett.* 269, 80–95. doi:10.1016/j.epsl.2008.01.051

Mattey, D., Fairchild, I. J., Atkinson, T. C., Latin, J., Ainsworth, M., and Durell, R. (2010). Seasonal microclimate control of calcite fabrics, stable isotopes and trace elements in modern speleothem from st michaels cave, Gibraltar. *Geochim. Cosmochim. Ac.* 336, 323–344. doi:10.1144/SP336.17

McGillen, M., and Fairchild, I. (2005). An experimental study of incongruent dissolution of $CaCO_3$ under analogue glacial conditions. *J. Glaciol.* 51, 383–390. doi:10.3189/172756505781829223

Mcmillan, E. A., Fairchild, I. J., Frisia, S., Borsato, A., and Mcdermott, F. (2005). Annual trace element cycles in calcite–aragonite speleothems: evidence of drought in

the Western mediterranean 1200–1100yrbp. *J. Quat. Sci.* 20, 423–433. doi:10.1002/jqs.943

Musgrove, M. L., and Banner, J. L. (2004). Controls on the spatial and temporal variability of vadose dripwater geochemistry: Edwards aquifer, central texas. *Geochim. Cosmochim. Ac.* 68, 1007–1020. doi:10.1016/j.gca.2003.08.014

Niu, X., Zhang, H., Li, H., Wang, J., Bao, Y., and Cheng, H. (2022). Spatial variation of precipitation in eastern China over the past 150 years based on speleothem multi-proxy analysis. *Quat. Int.* 622, 89–96. doi:10.1016/j.quaint.2022.02.018

Orland, I. J., Bar-Matthews, M., Kita, N. T., Ayalon, A., Matthews, A., and Valley, J. W. (2009). Climate deterioration in the eastern mediterranean as revealed by ion microprobe analysis of a speleothem that grew from 2.2 to 0.9 ka in soreq cave, israel. *Quat. Res.* 71, 27–35. doi:10.1016/j.yqres.2008.08.005

Orland, I. J., Bar-Matthews, M., Ayalon, A., Matthews, A., Kozdon, R., Ushikubo, T., et al. (2012). Seasonal resolution of eastern mediterranean climate change since 34 ka from a soreq cave speleothem. *Geochim. Cosmochim. Ac.* 89, 240–255. doi:10.1016/j.gca.2012.04.035

Orland, I. J., Burstyn, Y., Bar-Matthews, M., Kozdon, R., Ayalon, A., Matthews, A. ., et al. (2014). Seasonal climate signals (1990-2008) in a modern Soreq Cave stalagmite as revealed by high-resolution geochemical analysis. *Chem. Geol.* 363, 322–333. doi:10.1016/j.chemgeo.2013.11.011

Oster, J. L., Montañez, I. P., and Kelley, N. P. (2012). Response of a modern cave system to large seasonal precipitation variability. *Geochim. Cosmochim. Ac.* 91, 92–108. doi:10.1016/j.gca.2012.05.027

Rampelbergh, M. V., Verheyden, S., Allan, M., Quinif, Y., and Claeys, P. (2014a). A 500-year seasonally resolved $\delta^{18}O$ and $\delta^{13}C$, layer thickness and calcite aspect record from a speleothem deposited in the han-sur-lesse cave, Belgium. *Clim. Past. Discuss.* 10, 4149–4190. doi:10.5194/cpd-10-4149-2014

Rampelbergh, M. V., Verheyden, S., Allan, M., Quinif, Y., and Claeys, P. (2014b). Monitoring of a fast-growing speleothem site from the han-sur-lesse cave, Belgium, indicates equilibrium deposition of the seasonal $\delta^{18}O$ and $\delta^{13}C$ signals in the calcite. *Clim. Past.* 10, 1871–1885. doi:10.5194/cp-10-1871-2014

Reeder, R. J., and Rakovan, J. (1999). *Surface structural controls on trace element incorporation during crystal growth*. Springer Netherlands, 143–162. doi:10.1007/978-94-015-9179-96

Reeder, P., and Reeder, R. J. (1995). Relationship between surface structure, growth mechanism, and trace element incorporation in calcite. *Geochim. Cosmochim. Ac.* 59, 735–749. doi:10.1016/0016-7037(95)00004-J

Riechelmann, D., Schröder-Ritzrau, A., Scholz, D., Fohlmeister, J., Spötl, C., Richter, D. K., et al. (2011). Monitoring bunker cave (nw Germany): a prerequisite to interpret geochemical proxy data of speleothems from this site. *J. Hydrol.* 409, 682–695. doi:10.1016/j.jhydrol.2011.08.068

Riechelmann, D., Riechelmann, S., Wassenburg, J. A., Fohlmeister, J., Schöne, B. R., Jochum, K. P., et al. (2020). High-resolution proxy records from two simultaneously grown stalagmites from zoolithencave (southeastern Germany) and their potential for palaeoclimate reconstruction. *Geochem. Geophy. Geosys.* 21. doi:10.1029/2019GC008755

Roberts, M. S., Smart, P. L., and Baker, A. (1998). Annual trace element variations in a holocene speleothem. *Earth Planet. Sci. Lett.* 154, 237–246. doi:10.1016/S0012-821X(97)00116-7

Scott, M. J., Jones, M. N., Woof, C., and Tipping, E. (1998). Concentrations and fluxes of dissolved organic carbon in drainage water from an upland peat system. *Environ. Int.* 24, 537–546. doi:10.1016/S0160-4120(98)00043-9

Sinclair, D. J., Banner, J. L., Taylor, F. W., Partin, J., Jenson, J., Mylroie, J., et al. (2012). Magnesium and strontium systematics in tropical speleothems from the Western Pacific. *Chem. Geol.* 294, 1–17. doi:10.1016/j.chemgeo.2011.10.008

Sinclair, D. J. (2010). Two mathematical models of Mg and Sr partitioning into solution during incongruent calcite dissolution. *Chem. Geol.* 283, 119–133. doi:10.1016/j.chemgeo.2010.05.022

Tadros, C. V., Treble, P. C., Baker, A., Fairchild, I., Hankin, S., Roach, R., et al. (2016). ENSO–cave drip water hydrochemical relationship: a 7-year dataset from south-eastern Australia. *Hydrol. Earth Syst. Sci.* 20, 4625–4640. doi:10.5194/hess-20-4625-2016

Tadros, C. V., Treble, P. C., Baker, A., Hankin, S., and Roach, R. (2019). Cave drip water solutes in south-eastern Australia: constraining sources, sinks and processes. *Sci. Total Environ* 651, 2175–2186. doi:10.1016/j.scitotenv.2018.10.035

Tan, L., and Lin, F. (2020). Rings" of stalagmites. *J. Earth Environ.* 11, 456–459. doi:10.7515/JEE203008

Tan, L., An, Z., Huh, C. A., Cai, Y., Shen, C. C., Shiau, L. J., et al. (2014a). Cyclic precipitation variation on the Western loess plateau of China during the past four centuries. *Sci. Rep.* 4, 6381. doi:10.1038/srep06381

Tan, L., Shen, C. C., Cai, Y., Lo, L., Cheng, H., and An, Z. (2014b). Trace-element variations in an annually layered stalagmite as recorders of climatic changes and anthropogenic pollution in central China. *Quat. Res.* 81, 181–188. doi:10.1016/j.yqres.2013.12.001

Tan, L., Cai, Y., An, Z., Cheng, H., Shen, C., Sebastian, F. M., et al. (2015). A Chinese cave links climate change, social impacts, and human adaptation over the last 500 years. *Sci. Rep.* 5, 12284. doi:10.1038/srep12284

Tan, L., Zhang, H., Qin, S., and An, Z. (2013). Climatic and anthropogenic impacts on $\delta^{13}C$ variations in a stalagmite from central China. *Terr. Atmos. Ocean. Sci.* 24, 333–343. doi:10.3319/tao.2012.12.27.01(tt)

Tegen, I., and Dörr, H. (1996). Mobilization of cesium in organic rich soils: correlation with production of dissolved organic carbon. *Water Air Soil Poll.* 88, 133–144. doi:10.1007/BF00157418

Tian, Y., Zhang, H., Zhang, R., Zhang, F., Liang, Z., Cai, Y., et al. (2021). Seasonal and Inter-Annual Variations of Stable Isotopic Characteristics of Rainfall and Cave Water in Shennong Cave, Southeast China, and It's Paleoclimatic Implication. *Front. Earth Sci.* 9, 794762. doi:10.3389/feart.2021.794762

Tooth, A. F., and Fairchild, I. J. (2003). Soil and karst aquifer hydrological controls on the geochemical evolution of speleothem-forming drip waters, Crag Cave, southwest Ireland. *J. Hydrol.* 273, 51–68. doi:10.1016/S0022-1694(02)00349-9

Treble, P., Shelley, J., and Chappell, J. (2003). Comparison of high resolution sub-annual records of trace elements in a modern (1911–1992) speleothem with instrumental climate data from southwest Australia. *Earth Planet. Sci. Lett.* 216, 141–153. doi:10.1016/S0012-821X(03)00504-1

Treble, P. C., Fairchild, I. J., Griffiths, A., Baker, A., Meredith, K. T., Wood, A., et al. (2015). Impacts of cave air ventilation and in-cave prior calcite precipitation on golgotha cave dripwater chemistry, southwest Australia. *Quat. Sci. Rev.* 127, 61–72. doi:10.1016/j.quascirev.2015.06.001

Vansteenberge, S., Winter, N. J. D., Sinnesael, M., Verheyden, S., Goderis, S., Malderen, S. J. M. V., et al. (2020). Reconstructing seasonality through stable-isotope and trace-element analyses of the proserpine stalagmite, han-sur-lesse cave, Belgium: indications for climate-driven changes during the last 400 years. *Clim. Past.* 16, 141–160. doi:10.5194/CP-16-141-2020

Wang, B., and Lin, H. (2002). Rainy Season of the Asian - Pacific Summer Monsoon. *J. Clim.* 15, 386–398. doi:10.1175/1520-0442(2002)015<0386:RSOTAP>2.0.CO;2

Wang, L., Manzoni, S., Ravi, S., Riveros-Iregui, D., and Caylor, K. (2016). Dynamic interactions of ecohydrological and biogeochemical processes in water-limited systems. *Ecosphere* 6, art133–27. doi:10.1890/ES15-00122.1

Yadava, M., Ramesh, R., and Pant, G. (2004). Past monsoon rainfall variations in peninsular India recorded in a 331-year-old speleothem. *Holocene* 14, 517–524. doi:10.1191/0959683604hl728rp

Yoshimura, K., Kanamitsu, M., Noone, D., and Oki, T. (2008). Historical isotope simulation using reanalysis atmospheric data. *J. Geophy. Res.* 113, D19108. doi:10.1029/2008JD010074

Zhang, J., and Li, T. (2019). Seasonal and interannual variations of hydrochemical characteristics and stable isotopic compositions of drip waters in Furong Cave, southwest China based on 12 years' monitoring. *J. Hydrol.* 572, 40–50. doi:10.1016/j.jhydrol.2019.02.052

Zhang, H., Cai, Y., Tan, L., Cheng, H., Qin, S., An, Z., et al. (2015). Large variations of $\delta^{13}C$ values in stalagmites from southeastern China during historical times: implications for anthropogenic deforestation. *Boreas* 3, 511–525. doi:10.1111/bor.12112

Zhang, H., Cheng, H., Spötl, C., Cai, Y., Sinha, A., Tan, L., et al. (2018). A 200-year annually laminated stalagmite record of precipitation seasonality in southeastern China and its linkages to ENSO and PDO. *Sci. Rep.* 8, 12344. doi:10.1038/s41598-018-30112-6

Zhang, H. W., Brahim, Y. A., Li, H. Y., Zhao, J. Y., Kathayat, G., Tian, Y., et al. (2019). The Asian summer monsoon: Teleconnections and forcing mechanisms-A review from Chinese speleothem $\delta^{18}O$ records. *Quat* 2, 26. doi:10.3390/quat2030026

Zhang, H., Cheng, H., Cai, Y., Spötl, C., Sinha, A., Kathayat, G., et al. (2020). Effect of precipitation seasonality on annual oxygen isotopic composition in the area of spring persistent rain in southeastern China and its paleoclimatic implication. *Clim. Past.* 16, 211–225. doi:10.5194/cp-16-211-2020

Zhang, H., Zhang, X., Cai, Y., Sinha, A., Christoph, S., Baker, J., et al. (2021). A data-model comparison pinpoints holocene spatiotemporal pattern of east Asian summer monsoon. *Quat. Sci. Rev.* 261, 106911. doi:10.1016/j.quascirev.2021.106911

Zhang, H., Bao, Y., Zhang, R., Meng, B., Cai, Y., and Cheng, H. (2022). Characteristics and formation mechanism of stalagmite laminae in E'mei cave, Jiangxi Province, China. *Quat. Sci.* 42, 1148–1158. doi:10.11928/j.issn.1001-7410.2022.04.18

Zhou, T., Yu, R., Zhang, J., Drange, H., Cassou, C., Deser, C., et al. (2009). Why the Western Pacific subtropical high has extended westward since the late 1970s. *J. Clim.* 22, 2199–2215. doi:10.1175/2008JCLI2527.1

Zimmerman, U., Ehhalt, D., and Muennich, K. O. (1967). "Soil-water movement and evapotranspiration: changes in the isotopic composition of the water," in *Pp of isotopes in hydrology Vienna international atomic energy agency*, 567–584.